Explicit Stencil Computation Schemes Generated by Poisson's Formula for the 2D Wave Equation

Naum M. Khutoryansky
Department of Engineering Technology
Drexel University, Philadelphia, PA 19104, USA

April 5, 2019

A novel approach to building explicit stencil computation schemes for the transient 2D scalar wave equation is proposed and implemented. It is based on using the integral representation formula (Poisson's formula) that provides the exact solution $u(\mathbf{x},t)$ (where $\mathbf{x} \in \mathbb{R}^2$, t is time) of the initial-value problem for the transient 2D scalar wave equation at $t > 0$ through the initial conditions for both u and $v = \partial u / \partial t$. For the purpose of constructing a two-step time-marching algorithm, an additional integral representation formula for the sum $u(\mathbf{x},t_* + \tau) + u(\mathbf{x},t_* - \tau)$ is provided, with τ being a time step and $t_* \geq \tau$.

It is shown that integrals in the two representation formulas are easily calculated if the initial conditions and $u(\mathbf{x},t_*)$ as functions of spatial coordinates are approximated by stencil interpolation polynomials in the neighborhood of any point $\mathbf{x}_{ij}$ in a 2D Cartesian grid $\{(ih, jh), (i,j) \in \mathbb{Z}^2\}$ where h is a grid spacing.

As a result, if a uniform time grid $\{t_k = k\tau, k \in \mathbb{N}\}$ is chosen, the proposed time-marching algorithm consists of two numerical procedures: (a1) the calculation of $u(\mathbf{x}_{ij},t_1)$, at the very first time-step, through the initial values of both u and v at stencil nodes; (a2) the calculation of $u(\mathbf{x}_{ij},t_{n+1}), n \geq 1$, at the second and next time-steps, through a generated two-step scheme.

Three computational stencils (with 5, 9 and 13 space points) are built using the proposed approach. Their stability is discussed.

It is demonstrated by simulation that utilizing both procedures (a1) and (a2) are important for the accuracy of stencil computations, and that using the conventional first time-step calculation procedure instead of (a1) can lead to a significant loss of accuracy even for later time-steps.

1 Introduction

Stencil computations are widely implemented in many numerical algorithms that involve structured grids, including finite-difference (FD) techniques in such diverse areas as acoustics, fluid dynamics and electromagnetism. Standard FD formulas substitute

differential operators of the corresponding equations by values at a set of stencil nodes. Classical methods to compute the coefficients of weighted sum are mostly based on Taylor expansions. However, for stencils with multiple nodes including combinations of simpler stencils, the coefficients cannot be uniquely determined without additional conditions (see, e.g., [6]) which create competing finite-difference schemes for the same problem of interest and for the same set of stencil nodes.

In an explicit FD scheme, a solution value at each point in a time-space grid is calculated using a linear combination of values at its spatial neighbors from previous time steps. Among explicit FD schemes for the transient 2D wave equation the main attention in literature has been given to two-step schemes (which operate over three time levels t_{k+1}, t_k and t_{k-1}). They have been intensively studied and reviewed in many articles and books (see, e.g., [3, 6, 1, 2, 11, 8]).

Due to the availability of many competing finite-difference stencil schemes for the 2D wave equation, it is reasonable to consider building stencil computation schemes for this equation based on principles different from the finite-difference approximation of differential operators. If successful, such approaches can be useful not only for stencil calculations but also as additional tools to estimate efficiency of competing finite-difference schemes.

The three-level schemes pose some challenges when imposing the initial conditions. To calculate the value of u at the first time step $k = 1$, one needs information from steps $k = 0$ and $k = -1$. The initial condition for the solution u provides information at step k = 0. Any information at an earlier time must be inferred. The initial condition for $v = \partial u/\partial t$ can be used to do that. The conventional approach described in many textbooks (see, e.g., [11, 8]) uses the central difference for approximating that initial condition. For any point $\mathbf{x}$ in R^2, the value of $u(\mathbf{x},t_{-1})$ is inferred as $u(\mathbf{x},t_1) - 2\tau v(\mathbf{x},0)$. Even though this add-hoc approach is attractive due to its simplicity, it is worthwhile to consider the numerical schemes for both the first time step and the other steps in the framework of a unified approach.

This study focuses on utilizing the representation formula (Poisson's formula) to build some stencil computation schemes for the transient 2D scalar wave equation. As it is known, Poisson's formula gives the solution at any time point t as an integral of an expression that includes u and v at the initial time. Considering time $t_k, k \geq 1$, as the initial moment in Poisson's formula and using the polynomial interpolation of u at t_k in a central symmetric stencil, the value of u at the next time level t_{k+1} at the stencil center $\mathbf{x}$ is presented as a linear combination of the values of u at the stencil nodes at t_k minus $u(\mathbf{x},t_{k-1})$. A similar presentation is built for the first time level which includes instead of $u(\mathbf{x},t_{k-1})$ a linear combination of the values of v at the stencil nodes at $t = 0$. It is shown by simulation that even for the simplest 5-point stencil the proposed algorithm has an accuracy advantage in comparison with the conventional approach.

2 Representation formulas

Consider a Cauchy problem for the transient 2D scalar wave equation

$$\frac{\partial^2 u}{\partial t} - c^2\left(\frac{\partial^2 u}{\partial x_1^2} + \frac{\partial^2 u}{\partial x_2^2}\right) = 0, \quad u = u(\mathbf{x},t), \quad \mathbf{x} = (x_1,x_2) \text{ in } \mathbb{R}^2, \tag{1}$$

$$u|_{t=0} = u_0(\mathbf{x}), \quad \frac{\partial u}{\partial t}|_{t=0} = v_0(\mathbf{x}). \tag{2}$$

Its solution is given by the representation formula which is often named Poisson's formula for the 2D wave equation [4]:

$$u(\mathbf{x},t) = \frac{1}{2\pi ct^2} \int_{|\mathbf{y}-\mathbf{x}|^2<t^2} \frac{tu_0(\mathbf{y}) + t\ \nabla u_0(\mathbf{y}) \cdot (\mathbf{y}-\mathbf{x}) + t^2 v_0(\mathbf{y})}{\sqrt{c^2t^2 - |\mathbf{y}-\mathbf{x}|^2}} dy_1 dy_2 \tag{3}$$

where ∇ denotes the gradient operator and $\mathbf{y} = (y_1, y_2) \in \mathbb{R}^2$ is a variable of integration.

Rewriting the previous integral on the unit disk, we get

$$u(\mathbf{x},t) = \frac{1}{2\pi} \int_{|\mathbf{z}|<1} \frac{u_0(\mathbf{x}+ct\mathbf{z}) + ct\nabla u_0(\mathbf{x}+ct\mathbf{z}) \cdot \mathbf{z}}{\sqrt{1-|\mathbf{z}|^2}} dz_1 dz_2 + \frac{t}{2\pi} \int_{|\mathbf{z}|<1} \frac{v_0(\mathbf{x}+ct\mathbf{z})}{\sqrt{1-|\mathbf{z}|^2}} dz_1 dz_2 \tag{4}$$

where $\mathbf{z} = (z_1, z_2) \in \mathbb{R}^2$ is a new variable of integration.

Formulas (3) and (4) are also valid for negative t which can be proved based on the time reversal property of the wave equation. By substituting $-t$ for t in formula (4) and changing $\mathbf{z}$ to $-\mathbf{z}$ inside its integrals, we obtain the following analog of that formula for negative time:

$$u(\mathbf{x},-t) = \frac{1}{2\pi} \int_{|\mathbf{z}|<1} \frac{u_0(\mathbf{x}+ct\mathbf{z}) + ct\nabla u_0(\mathbf{x}+ct\mathbf{z}) \cdot \mathbf{z}}{\sqrt{1-|\mathbf{z}|^2}} dz_1 dz_2 - \frac{t}{2\pi} \int_{|\mathbf{z}|<1} \frac{v_0(\mathbf{x}+ct\mathbf{z})}{\sqrt{1-|\mathbf{z}|^2}} dz_1 dz_2 \tag{5}$$

The only difference between the right-hand sides of (4) and (5) is the opposite signs of the second term. So, we can eliminate this term by summing (4) and (5). Shifting the initial moment in the resulting formula from $t = 0$ to $t = t_*$, we get the following expression for a time increment τ:

$$u(\mathbf{x},t_*+\tau) + u(\mathbf{x},t_*-\tau) = \frac{1}{\pi} \int_{|\mathbf{z}|<1} \frac{u(\mathbf{x}+ct\mathbf{z},t_*) + ct\nabla u(\mathbf{x}+ct\mathbf{z},t_*) \cdot \mathbf{z}}{\sqrt{1-|\mathbf{z}|^2}} dz_1 dz_2 \tag{6}$$

where the right-hand side does not include the time derivative v.

Both formulas (4) and (6) will be used below to build a time-marching stencil computation algorithm for the wave equation.

3 The proposed time-stepping algorithm in the integral operator form

Consider a uniform time grid $\{t_0 = 0, t_1 = \tau, ..., t_k = k\tau, ...\}$ where τ is a fixed time-step. Denote by $u_k(\mathbf{x})$ the restriction of $u(\mathbf{x},t)$ to a moment $t = t_k$. Next, denote by $A(\mathbf{x},\tau)$ and $B(\mathbf{x},\tau)$ the following integral operators acting on continuous functions defined in $\mathbb{R}^2$:

$$A(\mathbf{x},\tau)f(\cdot) = \frac{1}{2\pi} \int_{|\mathbf{z}|<1} \frac{f(\mathbf{x}+c\tau\mathbf{z}) + c\tau\nabla f(\mathbf{x}+c\tau\mathbf{z}) \cdot \mathbf{z}}{\sqrt{1-|\mathbf{z}|^2}} dz_1 dz_2 \tag{7}$$

$$B(\mathbf{x},\tau)f(\cdot) = \frac{\tau}{2\pi} \int_{|\mathbf{z}|<1} \frac{f(\mathbf{x}+c\tau\mathbf{z})}{\sqrt{1-|\mathbf{z}|^2}} dz_1 dz_2 \tag{8}$$

The time-stepping algorithm proposed in this paper consists of two procedures based on the representation formulas (4) and (6):

1) *The procedure for the first time-step* which, according to (4), calculates $u_1(\mathbf{x})$ as

$$u_1(\mathbf{x}) = A(\mathbf{x},\tau)u_0(\cdot) + B(\mathbf{x},\tau)v_0(\cdot), \mathbf{x} \in \mathbb{R}^2 \tag{9}$$

2) *The procedure for the second and next time-steps* which, using (6) for $t_* = t_k$, calculates $u_{k+1}(\mathbf{x})$ as

$$u_{k+1}(\mathbf{x}) = 2A(\mathbf{x},\tau)u_k(\cdot) - u_{k-1}(\mathbf{x}), \mathbf{x} \in \mathbb{R}^2, k = 1,2,... \tag{10}$$

While formula (10) involves three time levels (two time-steps), formula (9) for the first time-step incorporates only two time levels (one time-step) without any finite difference approximation of the time derivative.

4 Using polynomial interpolation on stencils

Consider a two-dimensional uniform Cartesian grid $\{(ih, jh)\}$ where $(i, j) \in \mathbb{Z}^2$ is the grid point index and h is the grid spacing in both directions x_1 and x_2. Assume that the evaluation point $\mathbf{x}$ in formulas (9) and (10) is a grid point $\mathbf{x}_{ij}$. Our intention is to choose a stencil in the Cartesian grid and reduce the integral formulas (9) and (10) to linear combinations of the stencil node values of $u_k(\mathbf{x})$ $(k = 0,1,2,...)$ and $v_0(\mathbf{x})$. Such a reduction will be done by using polynomial interpolation.

Below, a stencil with m nodes chosen for interpolation is denoted by $\mathscr{S}_m(h)$. The corresponding index set $\{(q_1,q_2)\}$ is denoted by $\mathscr{Q}_m$. The stencil index components q_1 and q_2 are numbered relative to the referencing index $(0,0)$ of the stencil's center located at the evaluation point $\mathbf{x}_{ij}$. If the set $\mathscr{Q}_m$ is specified, then the stencil $\mathscr{S}_m(h)$ is determined as $\{\mathbf{x}_{q_1,q_2} = (q_1h, q_2h), (q_1,q_2) \in \mathscr{Q}_m\}$. So, polynomial interpolation in a neighborhood of the evaluation point $\mathbf{x}_{ij}$ will be carried out using interpolation points

$$\mathbf{x}_{i,j} + \mathbf{x}_{q_1,q_2} = \mathbf{x}_{i+q_1,j+q_2}, \quad (q_1,q_2) \in \mathscr{Q}_m \tag{11}$$

Following [9] we associate with $\mathscr{Q}_m$ a set of m distinct bivariate monomials

$$\mathscr{M}_m = \{x_1^{\alpha(q_1)} x_2^{\alpha(q_2)}\}, (q_1,q_2) \in \mathscr{Q}_m\} \tag{12}$$

where

$$\alpha(q) = \begin{cases} 2|q| - 1 & \text{if } q < 0 \\ 2q & \text{if } q \geq 0. \end{cases} \tag{13}$$

The corresponding set of pairs of exponents $\{(\alpha(q_1), \alpha(q_2)), (q_1,q_2) \in \mathscr{Q}_m\}$ is denoted by $\mathscr{E}_m$. The function (13) appearing in the above definition of $\mathscr{M}_m$ has a unique inverse function

$$q(\alpha) = (-1)^\alpha \left[\frac{\alpha+1}{2}\right] \tag{14}$$

where $[\cdot]$ is the whole part function.

Therefore, formula (12) creates a one-to-one correspondence between sets $\mathscr{Q}_m$ and $\mathscr{M}_m$ (or $\mathscr{E}_m$).

Consider a polynomial space spanned by the set $\mathscr{M}_m$. It will be denoted by $\mathscr{P}_m$. The set $\mathscr{M}_m$ is the monomial basis of polynomial space $\mathscr{P}_m$. We shall use only those

sets $\mathscr{Q}_m$ that provide the poisedness [10] of the Lagrange interpolation problem for $\mathscr{P}_m$. In this case, there exists a Lagrange basis for $\mathscr{P}_m$, and the monomial basis can be easily transformed to the Lagrange basis as described below.

Assume that there is an ordering imposed on the monomials in $\mathscr{M}_m$

$$\{\mu_1(\mathbf{x}),...,\mu_m(\mathbf{x})\}. \tag{15}$$

where $\mu_s(\mathbf{x}) = x_1^{\alpha_1}x_2^{\alpha_2}$ with $s = g(\alpha_1,\alpha_2)$ being a bijection between the set $\mathscr{E}_m$ and the sequence $\{1,...,m\}$ of positive natural numbers. The corresponding stencil nodes are numbered accordingly using (14), and the order number is put as a subindex in parentheses:

$$\{\mathbf{x}_{(1)},...,\mathbf{x}_{(m)}\}. \tag{16}$$

Thus, we can calculate the following matrix:

$$D = \left[\mu_s(\mathbf{x}_{(r)})\right]_{m\times m} \tag{17}$$

If this matrix is non-singular, i.e., $\det(D) \neq 0$, which can be easily checked for every chosen set $\mathscr{M}_m$, then the inverse matrix

$$C = [c_{sr}]_{m\times m} = D^{-1} \tag{18}$$

is calculated. Its components are used to express the Lagrange basis functions through the chosen set of monomials:

$$L_s(\mathbf{x}) = \sum_{r=1}^{m} c_{sr}\mu_r(\mathbf{x}), \quad s = 1,...,m. \tag{19}$$

Once the Lagrange basis is obtained, we again need two indexes to denote the Lagrange basis functions in accordance with the two index notation for grid points. Using the bijection $s = g(\alpha_1,\alpha_2)$ introduced above and function (13), the relationship between an index pair (q_1,q_2) and the corresponding ordinal number s is given by the following expression:

$$s = \gamma(q_1,q_2) = g(\alpha(q_1),\alpha(q_2)). \tag{20}$$

Therefore, introducing a new (two index) notation for the Lagrange basis functions

$$\phi_{q_1,q_2}(\mathbf{x}) = L_{\gamma(q_1,q_2)}(\mathbf{x}), \tag{21}$$

we get the interpolation formula for a continuous function $f(\mathbf{x})$ in the form

$$\tilde{f}(\mathbf{x}) = \sum_{(q_1,q_2)\in\mathscr{Q}_m} f_{i+q_1,j+q_2}\phi_{q_1q_2}(\mathbf{x}) \tag{22}$$

Even though different sets of monomials and ordering structures inside them can be used for building Lagrange bases, a particular ordering method for monomials with a gradual increase of the total degree should be useful.

Denote by $\mathscr{M}$ the set of all monomials $x_1^{\alpha_1}x_2^{\alpha_2}$, $(\alpha_1,\alpha_2)\in\mathbb{N}^2$, where $\mathbb{N}$ is the set of all natural numbers including 0. For each monomial $x_1^{\alpha_1}x_2^{\alpha_2}$, the corresponding ordinal number s will be assigned using the following function:

$$s = g(\alpha_1,\alpha_2) = \frac{(\alpha_1+\alpha_2)(\alpha_1+\alpha_2+1)}{2} + \begin{cases} \alpha_1-\alpha_2 & \text{if } \alpha_2 < \alpha_1, \\ \alpha_2-\alpha_1+1 & \text{if } \alpha_2 \geq \alpha_1. \end{cases} \tag{23}$$

It is easy to prove that the function (23) provides a bijection between $\mathscr{M}$ and the set $\mathbb{N}^*$ of all positive natural numbers with the usual ordering. The order induced by (23) uses the total degree as the first sorting parameter (similarly to the more common graded lexicographic order) while the difference between individual degrees with the same total degree is used as the next sorting variable.

The set $\mathscr{M}$ endowed with the order induced by (23) will be denoted by $\mathscr{M}^*$. It will be shown in section 6 that ordered subsets of monomials from $\mathscr{M}^*$ corresponding to initial segments $\{1,...,m\}$ of $\mathbb{N}^*$ and denoted below by $\mathscr{M}^*_{\leq m}$ play a useful role in building numerical schemes for some space stencils.

Example 1. Consider building the Lagrange basis for the space of complete second degree polynomials. In this case, the monomial basis sequence ordered according to (23) is as follows:

$$\mathscr{M}^*_{\leq 6} = \{1, x_1, x_2, x_1x_2, x_1^2, x_2^2\} \tag{24}$$

The corresponding interpolation stencil node sequence will be written as

$$\{(0,0),(-h,0),(0,-h),(-h,-h),(h,0),(0,h)\} \tag{25}$$

The index set $\mathscr{Q}_6$ for the stencil nodes is shown in Figure 1.

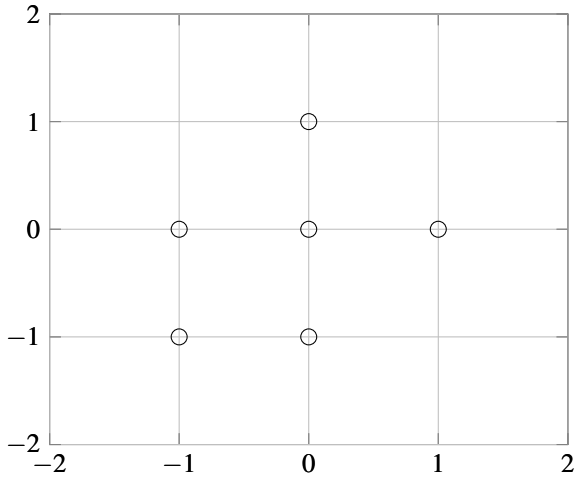

Figure 1: Index set for the interpolation 6-point stencil

Calculating matrix D we get

$$D = \begin{bmatrix} 1 & 1 & 1 & 1 & 1 & 1 \\ 0 & -h & 0 & -h & h & 0 \\ 0 & 0 & -h & -h & 0 & h \\ 0 & 0 & 0 & h^2 & 0 & 0 \\ 0 & h^2 & 0 & h^2 & h^2 & 0 \\ 0 & 0 & h^2 & h^2 & 0 & h^2 \end{bmatrix}$$

This matrix is non-singular with $\det(D) = 4h^8$. As a result, we get the Lagrange

basis as

$$\begin{gathered}\phi_{0,0}=L_1=1+\frac{x_1x_2}{h^2}-\frac{x_2^2}{h^2}-\frac{x_1^2}{h^2},\quad \phi_{-1,0}=L_2=-\frac{x_1}{2h}-\frac{x_1x_2}{h^2}+\frac{x_1^2}{2h^2},\\ \phi_{0,-1}=L_3=-\frac{x_2}{2h}-\frac{x_1x_2}{h^2}+\frac{x_2^2}{2h^2},\quad \phi_{-1,-1}=L_4=\frac{x_1x_2}{h^2},\\ \phi_{1,0}=L_5=\frac{x_1}{2h}+\frac{x_1^2}{2h^2},\quad \phi_{0,1}=L_6=\frac{x_2}{2h}+\frac{x_2^2}{2h^2}.\end{gathered}\tag{26}$$

One can see that the Lagrange basis (26) includes monomials in the scaled variables x_1/h and x_2/h with coefficients independent of h.

It is worth to mention here that node $(-h,h)$ will disappear in the corresponding numerical scheme (see section 6).

5 Calculating the integrals

The integrals in (7) and (8) can be calculated exactly if the function $f(\mathbf{y})$ is a polynomial in variables y_1 and y_2.

Without loss of generality, assume that the origin of the coordinate system is located at $\mathbf{x}$ which can be achieved by a parallel translation of the coordinate system. Let function $f(\mathbf{y})$ in (7) and (8), in accordance with (26), be a monomial in variables y_1/h and y_2/h

$$\mu(\mathbf{y})=\left(\frac{y_1}{h}\right)^{\alpha_1}\left(\frac{y_2}{h}\right)^{\alpha_2},\quad (\alpha_1,\alpha_2)\in\mathbb{N}^2.\tag{27}$$

Then the integrals in (7) and (8) will be expressed through the Courant number

$$\lambda=\frac{c\tau}{h}\tag{28}$$

Indeed, using the table of integrals of Gradshteyn & Ryzhik [5], expressions (7) and (8) are reduced to the following exact values:

$$A(0,\tau)\mu(\cdot)=0,\quad B(0,\tau)\mu(\cdot)=0\quad \text{if } \alpha_1 \text{ or } \alpha_2 \text{ are non-negative odd integers,}\tag{29}$$

$$\begin{gathered}A(0,\tau)\mu(\cdot)=\frac{(\alpha_1-1)!!(\alpha_2-1)!!}{(\alpha_1+\alpha_2-1)!!}\lambda^{\alpha_1+\alpha_2},\\ B(0,\tau)\mu(\cdot)=\frac{\tau}{\alpha_1+\alpha_2+1}A(0,\tau)\mu(\cdot)\\ \text{if } \alpha_1 \text{ and } \alpha_2 \text{ are both non-negative even integers}\end{gathered}\tag{30}$$

where $(\cdot)!!$ is the double factorial. It is assumed that $(-1)!!=1, 0!!=1$.

The above formulas allow one to exactly calculate integrals (7) and (8) when $f(\cdot)$ is a polynomial with respect to x_1 and x_2.

6 Particular stencil schemes

Now we can start building some stencil computation schemes by transforming the procedures (9) and (10) into algebraic expressions. All the functions $u_0(\mathbf{x}), v_0(\mathbf{x})$ and $u_k(\mathbf{x}), k=1,2,...$ included in these procedures will be interpolated in a stencil's center

neighborhood using the same stencil nodes. The following standard notations for grid values of the solution and initial conditions will be used in the computation schemes:

$$u_{ij}^0 = u(\mathbf{x}_{ij},0), v_{ij}^0 = v(\mathbf{x}_{ij},0), (i,j) \in \mathbb{Z}^2, \tag{31}$$

$$u_{ij}^k = u(\mathbf{x}_{ij},k\tau), k \in \mathbb{N}^*, (i,j) \in \mathbb{Z}^2. \tag{32}$$

6.1 The 5-point stencil

Consider the monomial basis (24) used in example 1 and the corresponding Lagrange basis (26). Using formulas from section 5 and notation (21) we get

$$\begin{aligned} A(0,\tau)\phi_{00}(\cdot) = 1-2\lambda^2, \quad A(0,\tau)\phi_{-1,-1}(\cdot) = 0, \\ A(0,\tau)\phi_{\pm1,0}(\cdot) = A(0,\tau)\phi_{0,\pm1}(\cdot) = \frac{1}{2}\lambda^2, \end{aligned} \tag{33}$$

$$\begin{aligned} B(0,\tau)\phi_{0,0}(\cdot) = \tau(1-\frac{2}{3}\lambda^2), \quad B(0,\tau)\phi_{-1,-1}(\cdot) = 0, \\ B(0,\tau)\phi_{\pm1,0}(\cdot) = B(0,\tau)\phi_{0,\pm1}(\cdot) = \frac{\tau}{6}\lambda^2, \end{aligned} \tag{34}$$

So, all coefficients for node $(-h,-h)$ disappear and the corresponding computational scheme contains only 5 spatial points which is shown in Figure 2.

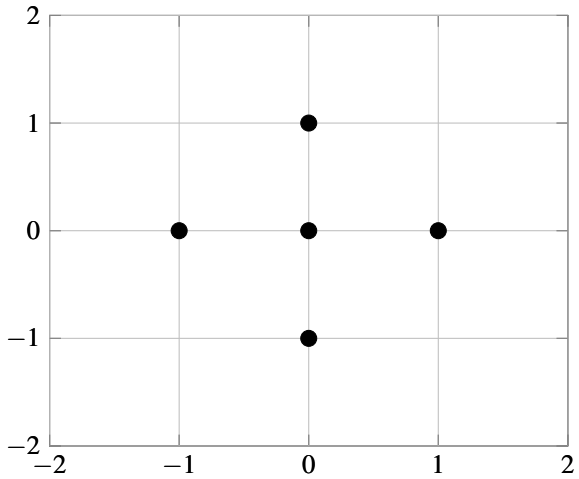

Figure 2: Index set for the computational 5-point scheme

6.1.1 A new first time-step expression

As a result, the proposed 5-point stencil computational scheme is as follows:
1) *for the first time-step*

$$u_{ij}^1 = u_{ij}^0 + \tau v_{ij}^0 + \frac{\lambda^2}{2}\left(u_{i-1,j}^0 + u_{i+1,j}^0 + u_{i,j-1}^0 + u_{i,j+1}^0 - 4u_{ij}^0\right) + \frac{\tau\lambda^2}{6}\left(v_{i-1,j}^0 + v_{i+1,j}^0 + v_{i,j-1}^0 + v_{i,j+1}^0 - 4v_{ij}^0\right); \quad (35)$$

2) *for the second and next time-steps*

$$u_{ij}^{k+1} = 2u_{ij}^k - u_{ij}^{k-1} + \lambda^2\left(u_{i-1,j}^k + u_{i+1,j}^k + u_{i,j-1}^k + u_{i,j+1}^k - 4u_{ij}^k\right), \quad k = 1,2,... \quad (36)$$

The conventional approach for the 5-point stencil described in many textbooks (see, e.g.,[8]) uses the same procedure (36) for the second and next time-steps. However, for the first time-step, the conventional approach uses another formula (rather than (35)) based on the central difference for approximating the initial condition for v combined with (36) for $k = 0$ (e.g., see [8]):

$$u_{ij}^1 = u_{ij}^0 + \tau v_{ij}^0 + \frac{\lambda^2}{2}\left(u_{i-1,j}^0 + u_{i+1,j}^0 + u_{i,j-1}^0 + u_{i,j+1}^0 - 4u_{ij}^0\right). \quad (37)$$

Comparing (35) and (37) one can see that the first three terms of the right-hand parts of these equations coincide, but the forth term present in the right-hand side of (35) is absent in (37).

The stability condition for both numerical schemes utilizing (36) is well known from von Neumann stability analysis [11]:

$$\lambda \le \lambda_{\max} = \frac{\sqrt{2}}{2}. \quad (38)$$

6.1.2 Standing wave simulation

To make a numerical comparison of both approaches, we shall use the initial and boundary conditions corresponding to a standing wave exact solution:

$$u_e(x_1,x_2,t) = \sin(2\pi x_1)\sin(2\pi x_2)\sin(2\sqrt{2}\pi ct). \quad (39)$$

This solution creates the following pair of initial conditions for the numerical simulation:

$$u(x_1,x_2,0) = 0, \quad v(x_1,x_2,0) = 2\sqrt{2}\pi c\ \sin(2\pi x_1)\sin(2\pi x_2). \quad (40)$$

We shall consider the unit square $\Omega = [0,1]^2$ as a space grid region for the numerical solution and use boundary condition $u = 0$ on $\partial\Omega$ generated by (39). In addition, we assume that $c = 1$ and consider a time grid interval of $[0, 2\lambda]$ for simulation.

The accuracy of both numerical schemes will be estimated using the relative L^2 error defined as

$$E(n,n_t) = \left(\frac{\sum_{k=1}^{n_t}\sum_{i=0}^{n}\sum_{j=0}^{n}\left(u_{ij}^k - u_e(ih,jh,k\tau)\right)^2}{\sum_{k=1}^{n_t}\sum_{i=0}^{n}\sum_{j=0}^{n}\left(u_e(ih,jh,k\tau)\right)^2}\right)^{1/2} \quad (41)$$

where n_t is the number of time-steps and n is the space discretization number related to h by equation $nh = 1$.

The relative L^2 errors for the proposed new 5-point scheme (35)&(36) (based on Poisson's formula) and the conventional one (37)&(36) will be denoted by $E_{P5}(n,n_t)$ and $E_{C5}(n,n_t)$, respectively. Calculated values of $E_{P5}(n,n_t)$, $E_{C5}(n,n_t)$ and their ratio for different combinations of n, n_t and $\lambda = 0.707$ are presented in table 1 below. For every value of n used, three values of n_t are considered: $n_t = 1$ (to check errors after the first step), $n_t = n$ and $n_t = 2n$ (to demonstrate the error accumulation process).

Table 1: Wave (39) simulations using the 5-point stencil.

n	n_t	λ	E_{P5}	E_{C5}	E_{C5}/E_{P5}
10	1	0.707	$9.0843\cdot10^{-4}$	$6.8938\cdot10^{-2}$	75.9
10	10	0.707	$9.1540\cdot10^{-4}$	$6.8945\cdot10^{-2}$	75.3
10	20	0.707	$9.1604\cdot10^{-4}$	$6.8945\cdot10^{-2}$	75.3
20	1	0.707	$5.4767\cdot10^{-5}$	$1.6636\cdot10^{-2}$	304
20	20	0.707	$5.6800\cdot10^{-5}$	$1.6638\cdot10^{-2}$	293
20	40	0.707	$5.7372\cdot10^{-5}$	$1.6638\cdot10^{-2}$	290
40	1	0.707	$3.3924\cdot10^{-6}$	$4.1230\cdot10^{-3}$	1215
40	40	0.707	$4.0331\cdot10^{-6}$	$4.1234\cdot10^{-3}$	1022
40	80	0.707	$4.4928\cdot10^{-6}$	$4.1234\cdot10^{-3}$	918
80	1	0.707	$2.1158\cdot10^{-7}$	$1.0285\cdot10^{-3}$	4861
80	80	0.707	$4.3820\cdot10^{-7}$	$1.0286\cdot10^{-3}$	2347
80	160	0.707	$6.5824\cdot10^{-7}$	$1.0286\cdot10^{-3}$	1563

Table 1 clearly shows that the practical accuracy of the new scheme is much higher than that of the conventional one with the error ratio $E_{C5}(n,n)/E_{P5}(n,n)$ exceeding 10^3 for more dense grids. So, using the conventional first time-step calculation procedure instead of the new one can lead to a significant loss of accuracy even for later time-steps. Increases of the relative L^2 errors from $n_t = n$ to $n_t = 2n$ are negligible (less than 10^{-6}).

6.1.3 Simulation of a trailing wave produced by a point impulse source

Another benchmark example that we shall simulate in the same space region $\Omega = [0,1]^2$ is a trailing wave solution for $t \geq 0$ corresponding to a point impulse source wave excited from the center of region $\Omega = [0,1]^2$ at a negative moment $t = -d$:

$$u_e(x_1,x_2,t) = \frac{1}{2\pi c}\frac{H(c(t+d)-r)}{\sqrt{c^2(t+d)^2-r^2}}, \quad r = \sqrt{(x_1-0.5)^2+(x_2-0.5)^2}, \qquad (42)$$

where $H(\cdot)$ is the Heaviside function and $d > 0$ is large enough to allow the corresponding wavefront to move outside of the region Ω before $t = 0$. This condition is satisfied if we assume that $cd > 1/\sqrt{2}$. Next, we suppose that the solution (42) specifies boundary values of $u(\mathbf{x},t)$ on $\partial\Omega$ and generates the following pair of initial conditions for the numerical simulation with $c = 1$:

$$u(x_1,x_2,0) = \frac{1}{2\pi\sqrt{d^2-r^2}}, \quad v(x_1,x_2,0) = \frac{-d}{2\pi(d^2-r^2)^{3/2}} \quad \text{in } \Omega. \qquad (43)$$

The resulting relative L^2 errors (41) for $d = 0.75$ are presented in Table 2. They show that the accuracy of the new scheme is approximately 10 times higher than that of the standard one.

Table 2: Wave (42) simulations using the 5-point stencil.

n	n_t	d	λ	E_{P5}	E_{C5}	E_{C5}/E_{P5}
10	10	0.75	0.707	$1.1478 \cdot 10^{-3}$	$1.1124 \cdot 10^{-2}$	9.69
20	20	0.75	0.707	$3.8221 \cdot 10^{-4}$	$3.8228 \cdot 10^{-3}$	10.0
40	40	0.75	0.707	$1.0799 \cdot 10^{-4}$	$1.1281 \cdot 10^{-3}$	10.4
80	80	0,75	0.707	$2.8379 \cdot 10^{-5}$	$3.0000 \cdot 10^{-4}$	10.6

6.2 A 9-point square stencil

Consider the initial segment $\mathscr{M}^*_{\leq 11}$ of $\mathscr{M}^*$ with the last member equal to $x_1^2 x_2^2$:

$$\{1, x_1, x_2, x_1x_2, x_1^2, x_2^2, x_1^2x_2, x_1x_2^2, x_1^3, x_2^3, x_1^2x_2^2\} \tag{44}$$

This set includes all the monomials of total degree ≤ 3 and one monomial $(x_1^2 x_2^2)$ of total degree $= 4$, and is the minimal initial segment of $\mathscr{M}^*$ that includes the bivariate tensor-product of the monomial bases for the second degree polynomials in each spatial coordinate. The corresponding index set $\mathscr{Q}_{11}$ is shown in Figure 3 where both solid dots and empty circles denote interpolation points. The corresponding Lagrange basis can be easily calculated using matrix (17) and presented similar to (26). However, it is preferable to avoid presenting long expressions that include 11 monomials and display only terms that will be used later. Denote by $\phi^e_{q_1,q_2}$ a part of ϕ_{q_1,q_2} that includes all the

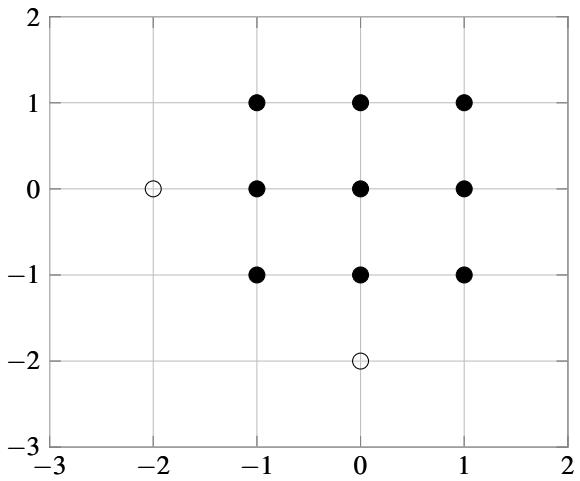

Figure 3: Index set for the 11-point interpolation stencil

monomial terms with even exponents in both coordinates. Then we get

$$\begin{gathered}\phi^e_{0,0}=1-\frac{x_1^2}{h^2}-\frac{x_2^2}{h^2}+\frac{x_1^2x_2^2}{h^4},\quad \phi^e_{-2,0}=\phi^e_{0,-2}=0,\\ \phi^e_{\pm1,0}=\frac{1}{2}\left(\frac{x_1^2}{h^2}-\frac{x_1^2x_2^2}{h^4}\right),\quad \phi^e_{0,\pm1}=\frac{1}{2}\left(\frac{x_2^2}{h^2}-\frac{x_1^2x_2^2}{h^4}\right),\quad \phi^e_{\pm1,\pm1}=\frac{1}{4}\frac{x_1^2x_2^2}{h^4}.\end{gathered} \tag{45}$$

6.2.1 A new 9-point time-stepping scheme

It follows from the results (29) and (30) of section 5 that functions $\phi^e_{q_1,q_2}$ rather than the complete Lagrange basis will be used in building numerical schemes. Therefore, two points (-2,0) and (0.-2) (presented by empty circles in Figure 3) will disappear in the corresponding numerical scheme. The remaining nodes (solid circles in Figure 3) create the 9-point square-shaped computational stencil. Using (29)-(30) we obtain:

$$\begin{gathered}A(0,\tau)\phi_{00}(\cdot)=1-2\lambda^2+\frac{\lambda^4}{3},\quad A(0,\tau)\phi_{\pm1,\pm1}(\cdot)=\frac{\lambda^4}{12},\\ A(0,\tau)\phi_{\pm1,0}(\cdot)=A(0,\tau)\phi_{0,\pm1}(\cdot)=\frac{\lambda^2}{2}-\frac{\lambda^4}{6},\end{gathered} \tag{46}$$

$$\begin{gathered}B(0,\tau)\phi_{00}(\cdot)=\tau\left(1-\frac{2\lambda^2}{3}+\frac{\lambda^4}{15}\right),\quad B(0,\tau)\phi_{\pm1,\pm1}(\cdot)=\frac{\tau\lambda^4}{60},\\ B(0,\tau)\phi_{\pm1,0}(\cdot)=B(0,\tau)\phi_{0,\pm1}(\cdot)=\frac{\tau\lambda^2}{6}\left(1-\frac{\lambda^2}{5}\right),\end{gathered} \tag{47}$$

Now we can use (9) and (10) to build a new 9-point numerical scheme similar to (35)-(36). However, to avoid writing long expressions, some additional notations will be needed:

$$\begin{gathered}\delta^k_{ij}(q_1,q_2)=u^k_{i+q_1,j+q_2}+u^k_{i-q_2,j+q_1}+u^k_{i1-q_1,j-q_2}+u^k_{i+q_2,j-q_1}-4u^k_{i,j},\\ \varepsilon^0_{ij}(q_1,q_2)=v^0_{i+q_1,j+q_2}+v^0_{i-q_2,j+q_1}+v^0_{i-q_1,j-q_2}+v^0_{i+q_2,j-q_1}-4v^0_{i,j},\\ k\in\mathbb{N},(q_1,q_2)\in\mathbb{N}^2.\end{gathered} \tag{48}$$

Thus, the following time-stepping numerical scheme is derived:

1) *for the first time-step*

$$\begin{aligned}u^1_{ij}=u^0_{ij}+\tau v^0_{ij}+\frac{\lambda^2}{2}\left[\left(1-\frac{\lambda^2}{3}\right)\delta^0_{ij}(1,0)+\frac{\lambda^2}{6}\delta^0_{ij}(1,1)\right]\\ +\frac{\tau\lambda^2}{6}\left[\left(1-\frac{\lambda^2}{5}\right)\varepsilon^0_{ij}(1,0)+\frac{\lambda^2}{10}\varepsilon^0_{ij}(1,1)\right];\end{aligned} \tag{49}$$

2) *for the second and next time-steps*

$$u^{k+1}_{ij}=2u^k_{ij}-u^{k-1}_{ij}+\lambda^2\left[\left(1-\frac{\lambda^2}{3}\right)\delta^k_{ij}(1,0)+\frac{\lambda^2}{6}\delta^k_{ij}(1,1)\right],\quad k=1,2,\ldots \tag{50}$$

The stability condition for the above numerical scheme can be easily obtained from von Neumann stability analysis [11]:

$$\lambda\le\lambda_{\max}=\frac{\sqrt{3-\sqrt{3}}}{2}\approx0.796. \tag{51}$$

To our knowledge this numerical scheme has not been presented previously in the literature. A conventional explicit nine-point square-shaped scheme (dubbed the isotropic scheme (see, e.g., [12]) has a different form obtained using a 9-point finite difference approximation of the Laplace operator in the two-dimensional space [7]:

$$u_{ij}^{k+1} = 2u_{ij}^{k} - u_{ij}^{k-1} + \lambda^2 \left[\frac{2}{3}\delta_{ij}^{k}(1,0) + \frac{1}{6}\delta_{ij}^{k}(1,1) \right], \quad k = 1,2,\ldots \tag{52}$$

Comparing the coefficients in (50) and (52) it is easy to see that the term $\delta_{ij}^{k}(1,1)$ is less influential in the new 9-point scheme than in the conventional 9-point scheme (with a coefficient ratio equal to λ^2). The stability condition for the conventional scheme is less restrictive than for the new one: $\lambda \leq \lambda_{\max} = \sqrt{3}/2 \approx 0.866$. On the other hand, the new scheme has some accuracy advantages in comparison with the conventional 9-point approach for $\lambda \leq 0.796$ which is shown in the next subsection.

6.2.2 Numerical simulation

We consider simulation results for the proposed 9-point scheme (49)-(50) using initial and boundary conditions generated by the exact solutions of the previous subsection. Let $c = 1$. We assume that the unit square $\Omega = [0,1]^2$ is used as a space grid region, the time grid interval is $[0,\lambda]$ with $n_t = n$. A comparison will be made with simulated results on the same grids for the conventional scheme (52). Even though no expression for the first time-step corresponding to the conventional 9-point scheme is presented in [12], the usual approach based on the central difference for approximating the initial condition for v combined with (52) provides the corresponding expression

$$u_{ij}^{1} = u_{ij}^{0} + \tau v_{ij}^{0} + \frac{\lambda^2}{2} \left[\frac{2}{3}\delta_{ij}^{0}(1,0) + \frac{1}{6}\delta_{ij}^{0}(1,1) \right] \tag{53}$$

that will be used for numerical simulation.

In addition, simulation results will be provided for the new scheme (50) but using instead of (49) the conventional approach based on the central difference for approximating the initial condition for v. The corresponding first time-step expression has the form

$$u_{ij}^{1} = u_{ij}^{0} + \tau v_{ij}^{0} + \frac{\lambda^2}{2} \left[\left(1 - \frac{\lambda^2}{3}\right) \delta_{ij}^{0}(1,0) + \frac{\lambda^2}{6}\delta_{ij}^{0}(1,1) \right] \tag{54}$$

which coincides with (49) if the fourth term in its right-hand side is omitted.

The simulation results are presented in the next two tables and cover both standing wave and trailing wave simulations. We use two values $\lambda = 0.707$ (as in Tables 1 and 2) and $\lambda = 0.796$ (based on the stability condition (51)) for the simulation. Relative L^2 errors for the schemes (49)&(50), (54)&(50) and (53)&(52) are denoted by E_{P9}, E_{CP9} and E_{C9}, respectively. According to the simulated data, the new scheme (49)&(50) appears to be more accurate than the other two schemes for both $\lambda = 0.707$ and $\lambda = 0.796$. A demonstrated higher accuracy of the scheme (49)&(50) in comparison with (54)&(50) emphasizes the importance of using the new first time-step procedure instead of the conventional one.

Comparisons of the obtained results with Tables 1 and 2 show that accuracy of the both 9-point schemes in the simulated cases for $\lambda = 0.707$ is much lower than that of the new 5-point scheme.

Table 3: Wave (39) simulations using 9-point stencils

n	n_t	λ	E_{P9}	E_{CP9}	E_{C9}
10	10	0.707	$3.7058 \cdot 10^{-2}$	$8.8235 \cdot 10^{-2}$	$1.1741 \cdot 10^{-1}$
10	10	0.796	$2.9587 \cdot 10^{-2}$	$9.6096 \cdot 10^{-2}$	$1.1241 \cdot 10^{-1}$
20	20	0.707	$8.9333 \cdot 10^{-3}$	$2.1304 \cdot 10^{-2}$	$2.8002 \cdot 10^{-2}$
20	20	0.796	$8.0697 \cdot 10^{-3}$	$2.3410 \cdot 10^{-2}$	$2.7523 \cdot 10^{-2}$
40	40	0.707	$2.3723 \cdot 10^{-3}$	$5.2683 \cdot 10^{-3}$	$6.8821 \cdot 10^{-3}$
40	40	0.796	$2.5737 \cdot 10^{-3}$	$5.8296 \cdot 10^{-3}$	$6.8668 \cdot 10^{-3}$
80	80	0.707	$7.5573 \cdot 10^{-4}$	$1.3119 \cdot 10^{-3}$	$1.7084 \cdot 10^{-3}$
80	80	0.796	$1.0274 \cdot 10^{-3}$	$1.4578 \cdot 10^{-3}$	$1.7187 \cdot 10^{-3}$

Table 4: Wave (42) simulations using 9-point stencils

n	n_t	d	λ	E_{P9}	E_{CP9}	E_{C9}
10	10	0.75	0.707	$2.6021 \cdot 10^{-3}$	$1.3156 \cdot 10^{-2}$	$1.5301 \cdot 10^{-2}$
10	10	0.75	0.796	$2.8906 \cdot 10^{-3}$	$1.7117 \cdot 10^{-2}$	$1.8658 \cdot 10^{-2}$
20	20	0.75	0.707	$8.9889 \cdot 10^{-4}$	$4.3569 \cdot 10^{-3}$	$4.9178 \cdot 10^{-3}$
20	20	0.75	0.796	$9.4873 \cdot 10^{-4}$	$5.5339 \cdot 10^{-3}$	$5.9647 \cdot 10^{-3}$
40	40	0.75	0.707	$2.9200 \cdot 10^{-4}$	$1.2557 \cdot 10^{-3}$	$1.3892 \cdot 10^{-3}$
40	40	0.75	0.796	$3.4821 \cdot 10^{-4}$	$1.5673 \cdot 10^{-3}$	$1.6650 \cdot 10^{-3}$
80	80	0.75	0.707	$1.0449 \cdot 10^{-4}$	$3.3019 \cdot 10^{-4}$	$3.6165 \cdot 10^{-4}$
80	80	0.75	0.796	$1.4901 \cdot 10^{-4}$	$4.0710 \cdot 10^{-4}$	$4.2991 \cdot 10^{-4}$

6.3 A 13-point stencil

The next numerical stencil will be based on complete bivariate interpolation polynomials of the fourth degree. Consider the initial segment $\mathscr{M}^*_{\leq 15}$ of $\mathscr{M}^*$:

$$\{1, x_1, x_2, x_1x_2, x_1^2, x_2^2, x_1^2x_2, x_1x_2^2, x_1^3, x_2^3, x_1^2x_2^2, x_1^3x_2, x_1x_2^3, x_1^4, x_2^4\} \tag{55}$$

This set includes all the monomials of total degree ≤ 4. The corresponding index set $\mathscr{Q}_{15}$ is presented in Figure 4 where both thirteen solid dots and two empty circles denote interpolation points.

After calculating the corresponding Lagrange basis (see section 4) and using (29)-(30), one can determine that all the coefficients in expressions (9)-(10) related to the two empty circles will disappear. As a result, we get a numerical scheme that involves the 13-point stencil (the solid dots in Figure 4). The notations (48) will be used in presenting the scheme to make the expressions more compact:

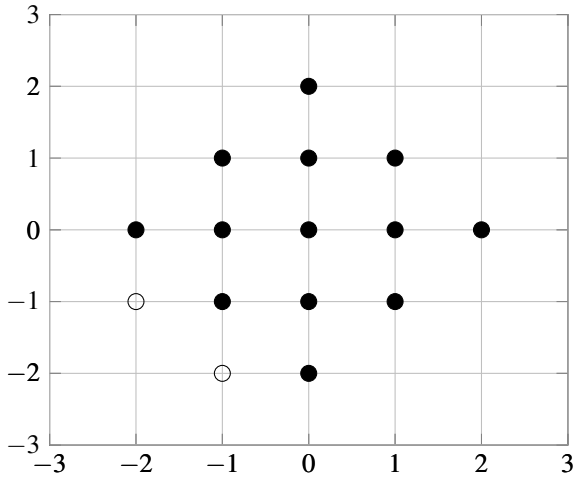

Figure 4: Index set for the 15-point interpolation stencil

1) *for the first time-step*

$$u_{ij}^1 = u_{ij}^0 + \tau v_{ij}^0 + \frac{\lambda^2}{2}\left[\frac{4-2\lambda^2}{3}\delta_{ij}^0(1,0) + \frac{\lambda^2}{6}\delta_{ij}^0(1,1) + \frac{\lambda^2-1}{12}\delta_{ij}^0(2,0)\right] + \frac{\tau\lambda^2}{6}\left[\left(\frac{4}{3} - \frac{2\lambda^2}{5}\right)\varepsilon_{ij}^0(1,0) + \frac{\lambda^2}{10}\varepsilon_{ij}^0(1,1) + \left(\frac{\lambda^2}{20} - \frac{1}{12}\right)\varepsilon_{ij}^0(2,0)\right]; \tag{56}$$

2) *for the second and next time-steps*

$$u_{ij}^{k+1} = 2u_{ij}^k - u_{ij}^{k-1} + \lambda^2\left[\frac{4-2\lambda^2}{3}\delta_{ij}^0(1,0) + \frac{\lambda^2}{6}\delta_{ij}^0(1,1) + \frac{\lambda^2-1}{12}\delta_{ij}^0(2,0)\right], \quad k = 1,2,\ldots \tag{57}$$

Formula (57) for the second and next time-steps is well-known [1, 2]. However, expression (56) for the first time-step has not been presented in the literature before.

An advantage of using this expression rather than the conventional one for the first time-step is shown in Table 5 where simulation results for the standing wave (39) solution are presented. The relative L^2 errors for the conventional and new approaches are denoted by E_{C13} and E_{P13}, respectively. For simplicity sake, the periodic boundary conditions were incorporated in the simulation taking into account that the solution (39) is periodic in both spatial directions. Since the maximal Courant number needed for stability of this scheme is $1/\sqrt{2}$, a value of $\lambda = 0.707$ was used.

The large values of the error ratio E_{C13}/E_{P13} demonstrated in Table 5 are explained by a higher accuracy of the new first time-step expression (56) in comparison with the conventional one for approximation of the initial condition for $\partial u/\partial t$. On the other hand, it is worth to notice that the relative L^2 error E_{C13} (corresponding to the conventional first time-step approach) in Table 5 has almost the same values as the error E_{C5} in Table 1 despite using a higher degree interpolation stencil in Table 5. That is, an error introduced at the first time-step probably suppresses advantages of using a higher degree interpolation at later time-steps.

Table 5: Wave (39) simulations using the 13-point stencil.

n	n_t	λ	E_{P13}	E_{C13}	E_{C13}/E_{P13}
10	10	0.707	$4.2146 \cdot 10^{-5}$	$6.8938 \cdot 10^{-2}$	$1.6357 \cdot 10^{3}$
20	20	0.707	$6.6004 \cdot 10^{-7}$	$1.6636 \cdot 10^{-2}$	$2.5205 \cdot 10^{4}$
40	40	0.707	$1.1471 \cdot 10^{-8}$	$4.1230 \cdot 10^{-3}$	$4.0537 \cdot 10^{5}$
80	80	0.707	$2.8884 \cdot 10^{-10}$	$1.0285 \cdot 10^{-3}$	$3.5608 \cdot 10^{6}$

7 Conclusion

A novel method is proposed to build explicit stencil computation schemes for the transient 2D scalar wave equation. The main idea is to use Poisson's formula that provides the exact solution of the initial-value problem through the initial conditions. Implementation of this formula together with polynomial stencil interpolation of the initial conditions creates two-step time-marching computation schemes and, additionally, new first time-step expressions different from those used in conventional FD methods.

Particular numerical schemes (with 5, 9 and 13 space points) are presented in the paper. A practical accuracy of them is checked on some benchmark problems that have exact solutions. It is demonstrated by simulation that the proposed computation approach can have some accuracy advantage in comparison with conventional finite difference schemes which is mostly attributed to the new first time-step expressions.

References

[1] G. Cohen. and P. Joly. Description and analysis of schemes, fourth-order in time and space, for 1-D and 2-D acoustic equations. *SEG Technical Program Expanded Abstracts 1987*, 527–530. Society of Exploration Geophysicists, 1987.

[2] G. Cohen. and P. Joly. Construction analysis of fourth-order finite difference schemes for the acoustic wave equation in nonhomogeneous media. *SIAM Journal on Numerical Analysis*, 33.4: 1266-1302, 1996.

[3] M.A. Dablain. The application of high-order differencing to the scalar wave equation. *Geophysics*, 51(1):54–66, 1986.

[4] L.C. Evans. *Partial Differential Equations*. American Mathematical Society, 1998.

[5] I.S. Gradshteyn and I.M. Ryzhik. *Table of integrals, series, and products*. Academic press, New York, 1965.

[6] O. Holberg. Computational aspects of the choice of operator and sampling interval for numerical differentiation in large-scale simulation of wave phenomena. *Geophysical prospecting*, 35(6):629–655, 1987.

[7] L.V. Kantorovich and V.I. Krylov. *Approximate methods of higher analysis*. Interscience Publishers, New York,, 1958.

[8] H.P. Langtangen and S. Linge. *Finite difference computing with PDEs : a modern software approach*. Texts in computational science and engineering, Vol. 16, Springer International Pub., New York, NY, 2017.

[9] E.H. McKinney. Generalized recursive multivariate interpolation. *Mathematics of Computation*, 26(119):723–735, 1972.

[10] T. Sauer and Y. Xu. On multivariate lagrange interpolation. *Mathematics of Computation*, 64(211):1147–1170, 1995.

[11] J.C. Strikwerda. *Finite difference schemes and partial differential equations*. Society for Industrial and Applied Mathematics, Philadelphia, 2nd edition, 2004.

[12] L.N. Trefethen. Group velocity in finite difference schemes. *SIAM Review*, 24(2):113–136, 1982.